Sub-damage-threshold plasma etching and profile tailoring of Si through laser-stimulated thermal desorption

Jason A. Peck, and David N. Ruzic

Citation: Journal of Vacuum Science & Technology A **36**, 021301 (2018); doi: 10.1116/1.4991586
View online: https://doi.org/10.1116/1.4991586
View Table of Contents: http://avs.scitation.org/toc/jva/36/2
Published by the American Vacuum Society

Articles you may be interested in

Role of the dense amorphous carbon layer in photoresist etching
Journal of Vacuum Science & Technology A: Vacuum, Surfaces, and Films **36**, 021304 (2018); 10.1116/1.5009640

Predicting synergy in atomic layer etching
Journal of Vacuum Science & Technology A: Vacuum, Surfaces, and Films **35**, 05C302 (2017); 10.1116/1.4979019

Thermal adsorption-enhanced atomic layer etching of Si_3N_4
Journal of Vacuum Science & Technology A **36**, 01B104 (2018); 10.1116/1.5003271

Etching low-k films by F atoms: Inside view
Journal of Vacuum Science & Technology A: Vacuum, Surfaces, and Films **36**, 02C103 (2018); 10.1116/1.5003890

Applying sputtering theory to directional atomic layer etching
Journal of Vacuum Science & Technology A: Vacuum, Surfaces, and Films **36**, 01B105 (2018); 10.1116/1.5003393

Graphene as plasma-compatible blocking layer material for area-selective atomic layer deposition: A feasibility study for III-nitrides
Journal of Vacuum Science & Technology A: Vacuum, Surfaces, and Films **36**, 01A107 (2018); 10.1116/1.5003421

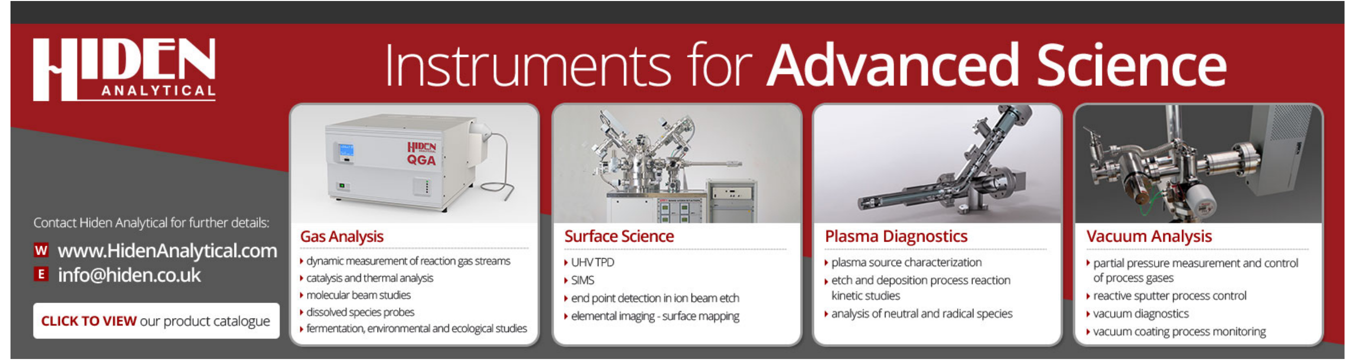

Sub-damage-threshold plasma etching and profile tailoring of Si through laser-stimulated thermal desorption

Jason A. Peck and David N. Ruzic[a)]
Department of Nuclear, Plasma, and Radiological Engineering, University of Illinois Urbana-Champaign, 104 S. Wright St., Urbana, Illinois 61801

(Received 22 June 2017; accepted 3 November 2017; published 28 November 2017)

A laser-assisted plasma etch process is presented as an alternative to reactive ion etching for Si wafer processing in upcoming integrated circuit technology nodes. Poly-Si films were etched using an upstream 13.56 MHz inductively coupled plasma source while simultaneously being exposed to a pulsed Nd:YAG laser using the 532 nm line, with 100 Hz and 7 ns Gaussian pulse duration. For a fluorocarbon etch recipe of 50:8 sccm Ar:C_4F_8 with varied O_2 flow, a minimum laser intensity for etch onset was necessary to overcome CF_x polymer deposition in the absence of substrate bias. This etch onset occurred at 20 ± 3 mJ/cm^2/pulse for 0 sccm O_2 flow, dropping to 8 ± 2 mJ/cm^2/pulse for 1.5 sccm O_2. Beyond this onset, the etch rate increased linearly with laser intensity. Secondary ion mass spectroscopy depth profiling data showed that the no-bias 532 nm laser-assisted etch process preserved the distinction between the Si surface and the CF_x polymer, with minimal uptake of etch gas residuals (C/F/O) in the Si. On the other hand, RIE showed significant straggle of the Si layer, spreading 3.5 nm through the CF_x polymer layer at 1.0 W/cm^2 radio-frequency bias and -140 V direct self-bias. COMSOL modeling of 532 nm incident on 22 nm half-pitch trench features showed strong polarization dependence, with deep-trench heating possible with polarization perpendicular to the trench line. This effect was confirmed in brief laser-assisted SF_6 etching of pre-existing 50 nm half-pitch linear trenches. *Published by the AVS.*
https://doi.org/10.1116/1.4991586

I. INTRODUCTION

The manufacturing of integrated circuits relies heavily on etching—removing material on a wafer based on the stencil produced by lithography.[1] With the 6+ decade trend of progressively decreasing feature size according to Moore's law,[2] the next-generation technology nodes of 7 and 5 nm present several challenges. Specifically relevant to etch, these include reliably etching smaller features and preserving surface fidelity.[3] The high energy of ions in reactive ion etching (RIE) is a key culprit in causing surface disorder and material mixing. With damage of even 1 nm in depth, this can be detrimental to the performance of a device in upcoming technology nodes.

This work proposes a new etch process, combining the traditional etch plasma with light exposure of the wafer as an alternative to the typical ion energy component. Like ions, light may be directed to target a specific surface, producing an anisotropic etch. Low average power is a key goal, as cost, scalability, and thermal budget are all concerns for incorporation into an industrial process. Light also has the advantage of differential absorption leading to selectivity and being able to be guided by regular features on a chip depending on its polarization leading to a here-to-fore impossible selectivity between horizontal and vertical patterns. Furthermore defocused light from a laser is independent of the plasma itself and could be directed to specific dies or regions of dies by digital light projection technology.

Many groups have explored the possibility of initiating or enhancing semiconductor etch with light exposure, though most primarily focused on UV sources due to their photolytic effect and high opacity to most materials. In fact, Shin *et al.*[4] showed that subthreshold removal of Si etch products could occur through the native vacuum ultraviolet emission (Ar 104.8, 106.6 nm lines) in the plasma itself. Etching of Si was observed in plasma-less conditions with both reactive (Cl_2)[5–7] and chemisorbed (NF_3, SF_6)[8,9] gases, in wet etching conditions,[10,11] and in plasma discharges such as CF_4/O_2 (Ref. 12) or Cl_2/Ar (Ref. 13) Sesselmann[6] showed three distinct regions of chemical etching stimulated by pulsed UV excimer lasers (248 nm KrF and 308 nm XeCl), with desorption peaking at 0.01–0.03 Å/pulse removal at 400–600 mJ/cm^2/pulse intensity before transitioning into ablation. Maki and Ehrlich[14] presented a candidate process for atomic layer etching (ALE) by using 193 nm ArF laser to desorb Cl-saturated GaAs without gas cycling, while Ishii *et al.*[15] demonstrated the efficacy of ALE via 248 nm KrF in the same chemistry. With regard to the laser's ability to structure materials, Choy and Cheah[10] saw applications in the formation of porous silicon, while Riedel *et al.*[9] produced conical micropatterning according to the laser speckle pattern.

Only a few researchers focused on visible light[5,11,12] (514.5 nm Ar^+ or frequency-doubled Yb) with etch enhancement attributed to thermal heating causing desorption of surface species. Holber's[12] tests with continuous-wave Ar^+ 514.5 nm in $CF_4 + O_2$ discharge showed local etch enhancement in Si, but the sustained heating to produce a temperature gradient in Si was wasteful and adverse to temperature-sensitive applications. Here, the use of visible light is to

[a)]Author to whom correspondence should be addressed; electronic mail: druzic@illinois.edu

produce selectivity based on the absorption characteristics: SiO_2 is transparent while Si, most hard masks and polymer resists are not.

Out of the slim body of research that exists, none pursued etching features of 100 nm or less, and the possibility of damage-free, low-thermal-budget, anisotropic etching was of auxiliary importance. Observed etch rate increases due to the introduction of a laser were also low compared to the requirements of the time, and thus the application was discarded as a viable processing step. With etch depths significantly lower and the restrictions on atomic surface fidelity higher than ever, laser-assisted plasma etching was revisited in this work. Initial studies were conducted in 2012 leading to a patent.[16] Complete details of this work can be found in Jason Peck's Ph.D. thesis.[17]

II. EXPERIMENTAL APPARATUS

Testing of the combination of pulsed visible laser exposure and plasma etching was conducted in a 10 in. Conflat cross with an upstream 13.56 MHz inductively coupled plasma (ICP) source to supply etch radicals and ions with density independent of sheath potential. A water-cooled substrate with optional 13.56 MHz RF bias and linear motion allowed for control of both plasma density and ion energy arriving at the sample surface. Si samples were placed on an anodized aluminum chuck and mounted to the substrate via load lock and transfer arm (Fig. 1).

Typical etch recipes involved a combination of C_4F_8 fluorocarbon etch gas, Ar buffer, and O_2 for polymer thinning. A fill pressure of 10 mTorr was used, controlled by 100 sccm Celerity Unit 1661 mass flow controllers, and determined by a Pfeiffer capacitance manometer.

In tandem with the etch plasma, a Nd:YAG pulsed laser was used to expose the poly-Si samples to 532 nm (second harmonic), pulsed at 100 Hz with a 7 ns Gaussian profile with a beam diameter of ∼1 cm. Vibrational dithering of the optics was used to mitigate the effect of the laser speckle. The per-pulse power output was measured with a Spectra-Physics bolometer.

III. RESULTS AND DISCUSSION

A. Etch activation and intensity trends

Inhibitor etch involving fluorocarbons relies on a CF_x polymer layer to build up on the feature sidewalls, while directed ion bombardment sputters away the soft polymer from the surface targeted for etching. To keep the polymer thin enough to prevent excessive buildup/saturation, an ashing gas such as O_2 is added to the plasma to thin the polymer. For a polymer-rich recipe of 50:8:1.5 sccm $Ar/C_4F_8/O_2$, no etch rate on Si was observed in the absence of substrate bias. This verge-of-etching baseline condition was the starting point for testing the etch enhancement introduced by pulsed (7 ns, 100 Hz) laser exposure at 532 nm.

As demonstrated in previous work through dopant ramping tests and XPS surface characterization (in press[18]) the synergy between visible (532 nm) laser exposure and the etch plasma on Si relies on instantaneous surface heating by

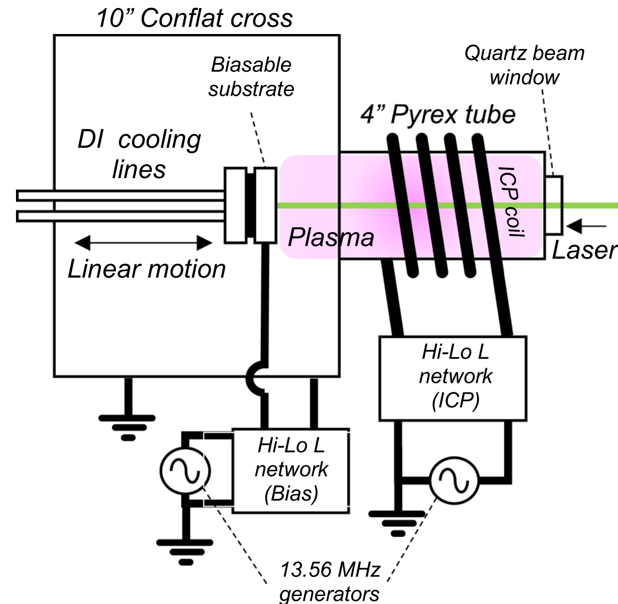

Fig. 1. (Color online) Upstream ICP etcher configuration with translateable, water-cooled, and biasable substrate. The ICP coil wound around a 4 in. Pyrex tube, excited plasma through a 13.56 MHz RF generator, and was matched via L-type matching network. A quartz window on the opposite end of the Pyrex tube permitted Process gases were regulated by 100 sccm mass flow controllers and injected through an inlet in the beam window.

the pulsed laser. With the laser desorbing involatile etch products (SiF, SiF_2, and SiF_3), the surface is cleared for new reaction sites. The instantaneous heating of the pulsed Nd:YAG laser was calculated to produce a significant rise in surface temperature with each pulse, e.g., 160 °C maximum rise at 40 mJ/cm^2/pulse 532 nm with a thermal decay time of ∼100 ns.

An increasing trend of etch rate with laser intensity was shown on poly-Si, as seen in Fig. 2. Etch activation depended on the presence of O_2, with onset at 20 mJ/cm with no O_2 flow, falling to 8 mJ/cm^2/pulse with 1.5 sccm O_2. This shift was shown to be caused by a thinner steady-state polymer layer, manifesting as a higher minimum laser intensity required to desorb the CF_x inhibitor and etch the underlying Si. Beyond this minimum intensity, laser etch enhancement increased roughly linearly for both cases.

B. SIMS determination of surface damage

With laser-assisted etch rates shown for fluorocarbon chemistry, high-resolution SIMS depth profiling was carried out to determine surface damage postlaser exposure when used as an alternative to ion bombardment. A 50:8:1.5 sccm $Ar/C_4F_8/O_2$ recipe was chosen for testing, as the O_2 content was just enough to produce a zero etch rate in the absence of either substrate bias or pulsed laser exposure. A baseline profile of a postetch surface, saturated with CF_x polymer, is shown in Fig. 3.

The surface postplasma in Fig. 3 shows a saturated surface of oxygenated CF_x polymer of roughly 3.5 nm thickness and 1:2 C/F ratio reflective of the etch gas, followed by an interlayer of 1–2 nm of the etch gas residuals diffusing into the wafer. A heightened O signal was seen in the Si surface

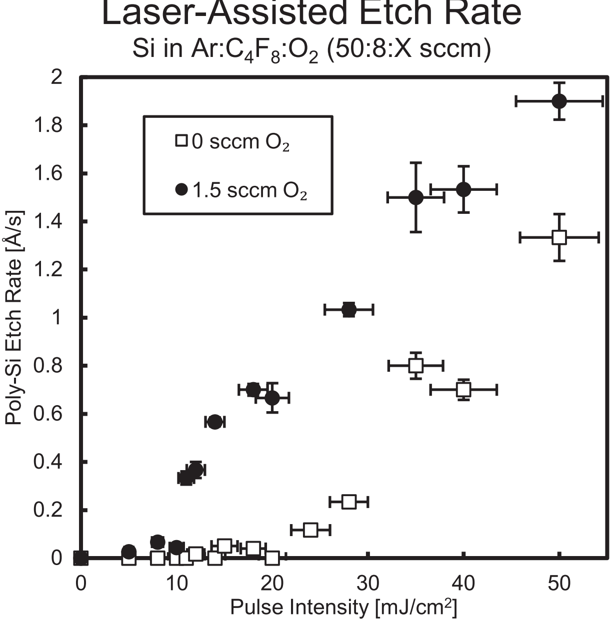

FIG. 2. Poly-Si etch rate in 50:8 sccm Ar:C_4F_8 for 0 and 1.5 sccm O_2 flow, plotted against Nd:YAG 532 nm pulse energy at 100 Hz, 7 ns pulse width. The configuration used was a downstream ICP etcher with 300 W of 13.56 MHz RF. Baseline etch rate is 0 in both cases due to the absence of substrate bias.

at 3.7 nm, presumably due to the presence of a thin native oxide. Alternatively, it may be due to higher reactivity of halogens with Si, a trait made apparent by the slight peak in the F signal which simultaneously occurs at 3.6 nm.

This barely zero etch rate recipe was then subjected to either ion bombardment (via RF-biased substrate) or pulsed 532 nm Nd:YAG at 100 Hz with 7 ns pulse width. The resultant depth profiles are shown in Fig. 4.

The ion bombardment trend in Fig. 4, with Fig. 4(c)'s 40 W bias corresponding to 360 V peak-to-peak and −140 V DC self-bias, shows the effect of ion damage on the Si

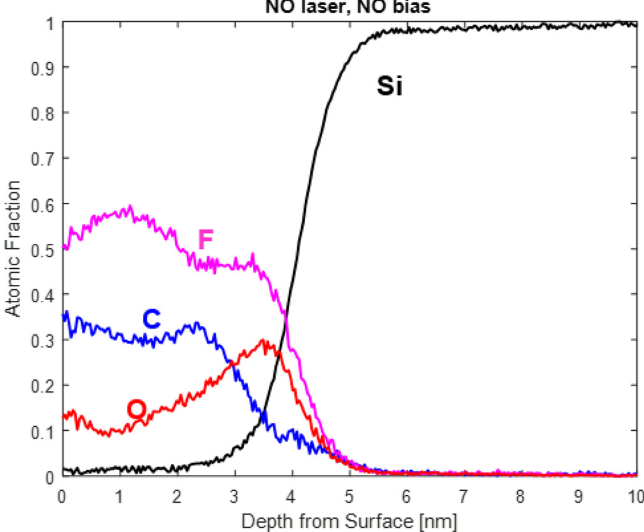

FIG. 3. (Color online) SIMS depth profile of a lightly etched Si surface using 50:8:1.5 sccm Ar/C_4F_8/O_2 at 10 mTorr, 300 W RF ICP, with no substrate bias and no laser exposure.

surface under fluorocarbon etch conditions. Rather than the distinct separation of the CF_x polymer and the polished Si wafer, ion-induced disorder has, instead, produced mixing of Si into the thinned CF_x barrier. With a thinner polymer inhibitor and forced migration of Si to the surface, etch onset occurs and increases proportional to the substrate bias power. However, etch gas residuals encroach much farther into the wafer, resulting in as much as 3 nm of penetration, coinciding with projected TRIM ion ranges of these atoms in Si.[19,20]

Alternatively, pulsed visible light exposure at 532 nm preserved the fidelity of the Si surface, exclusively thinning the CF_x polymer layer, going from an unexposed 3.5 ± 0.2 to 2.6 ± 0.2 nm at 20 mJ/cm^2/pulse and 2.0 ± 0.2 nm at 40 mJ/cm^2/pulse. Despite a much lower etch rate enhancement than ion bombardment at similar average areal power, the distinction between CF_x and Si remained, giving a hopeful chance of mitigating material damage and increasing residue removal postetch. The etch mechanism in the laser exposure case seems to be purely based on instantaneous heating causing polymer desorption, leaving out the surface mixing which occurs in the ion bombardment case.

These layer thickness trends are shown for RF substrate bias in Fig. 5 and for 532 nm pulsed laser exposure in Fig. 6. A key takeaway in the comparison between the two is that, while both methods thin the CF_x polymer layer, only laser exposure preserves the Si surface while ion bombardment increasingly expands it. The Si straggle saturates with increasing laser intensity (Fig. 6) while it continues to increase with increasing ion bombardment energy (Fig. 5). This mixing is similarly apparent in the increasing SiF_y interlayer thickness in Fig. 5, denoting significant residue uptake into the Si compared to the laser exposure case of Fig. 6. While the etch rate of the laser-induced removal was on the order of 0.1 nm/s and the etch rate of the ion-bombardment was five to ten times greater, the interlayer mixing and subsurface damage is not due to etch rate. These rates are all way below the flux level needed for overlapping damage cascades – only one event is happening at a time. RIE rates are proportional to the ion energy flux and removal occurs due to the ion bombardment breaking bonds and rearranging atoms. This occurs independently of rate–damage is inherent to the process itself. Light absorption leading to laser-induced removal has dramatically smaller momentum transfer and therefore does not rearrange the subsurface atoms resulting in less damage.

C. Trench heating simulations and 2D etch results

With promising results from SIMS on showing the laser's advantage over ion bombardment in reducing surface damage, an application of the laser-assisted etch process was necessary to prove visible light was capable of producing an anisotropic etch in the absence of energetic ion bombardment.

The leading question was whether a laser with wavelength much larger than the pattern's feature size could adequately heat the base of a rectangular trench line. To predict this, COMSOL simulations were carried out of a typical 22 nm

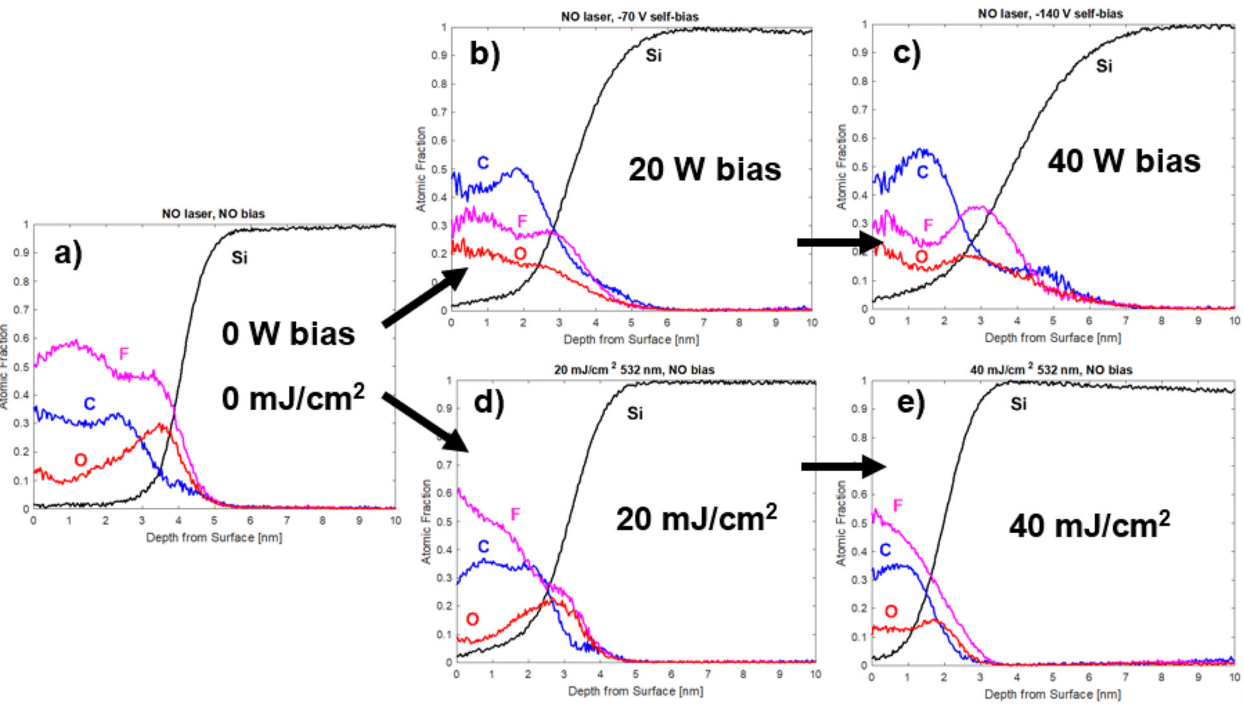

FIG. 4. (Color online) SIMS depth profile of the (a) no laser/no plasma control test, branching off into (b) 20 W and (c) 40 W (13.56 MHz RF) substrate bias, and (d) 20 mJ/cm^2 and (e) 40 mJ/cm^2 per pulse 532 nm Nd:YAG exposure. Tests were performed at room temperature.

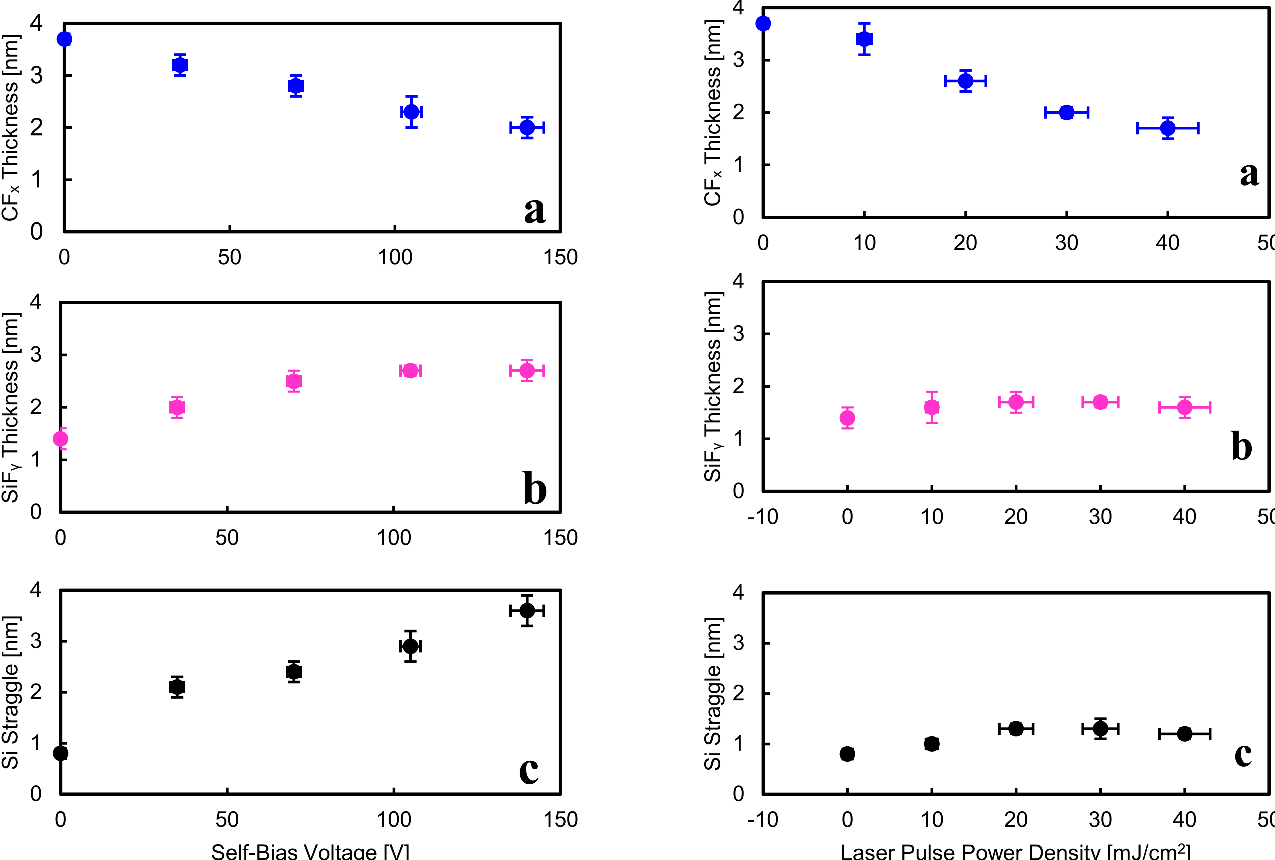

FIG. 5. (Color online) Substrate bias trends—(a) estimated layer thickness of CF_x surface polymer, (b) SiF_x interlayer, and (c) straggle/spread of etched Si in 50:8:1.5 sccm $Ar/C_4F_8/O_2$ at 10 mTorr with 300 W upstream ICP and RF-biased substrate of varying power (0–40 W, in 10 W increments) and no laser exposure.

FIG. 6. (Color online) Laser pulse intensity trends—(a) estimated layer thickness of CF_x, (b) SiF_y, and (c) Si straggle/spread of etched Si in 50:8:1.5 sccm $Ar/C_4F_8/O_2$ at 10 mTorr with 300 W upstream ICP and no substrate bias aside from the native plasma sheath, with 100 Hz pulsed Nd:YAG laser exposure at 532 nm up to 40 mJ/cm^2/pulse.

half-pitch trench line in Si, exposed to a surface-normal 532 nm plane wave.

Interestingly, the trench structure itself behaved as a polarization-selective waveguide, showing an in-trench wavelength of roughly 370 nm when polarization is perpendicular to the trench line, falling between the vacuum wavelength ($\lambda_o = 532$ nm) and the wavelength in Si ($n_{\mathrm{Si},\,532\,\mathrm{nm}} = 4.14$, $\lambda_{\mathrm{Si},\,532\,\mathrm{nm}} = 129$ nm), from Jellison.[20] This polarization condition shows deep trench light delivery, even at modeled aspect ratios of 80, as shown in Fig. 7(a). However, when polarization is parallel to the trench line, as shown in Fig. 7(b), in-trench propagation does not occur. The resistive heating due to the incident wave is plotted for each polarization in Fig. 8.

With an understanding of the polarization dependence of light incident on a trench line with feature size $\ll \lambda_o$, the laser-assisted etch process was tested on a Si linear trench pattern of 60 nm critical dimension and 120 nm depth. The existing structure was subjected to a brief (60 s), dilute (50:1 sccm) Ar/SF_6 etch with no bias with the substrate 12 cm downstream from a 100 W 13.56 MHz ICP discharge. Ar/SF_6 was used as opposed to the Ar/C_4F_8/O_2 recipe to directly show the difference without the need for an ashing step to remove the inhibitor layer. The evolution of the

FIG. 7. (Color online) Frequency domain simulations of a 532 nm beam incident on a 22 nm half-pitch, nine trench array with AR = 80. (a) $|E_x|$ (polarization $\perp$ to the trench line, horizontal) and (b) $|E_z|$ ($\parallel$ to the trench line, out of page) are plotted. Trenches were finely meshed with six elements per opening. The geometry was made with perfectly matched layers in y and periodic in x, hence the overlapping interference patterns in the bulk Si. Fields correspond to a 1 W/cm^2 laser fluence.

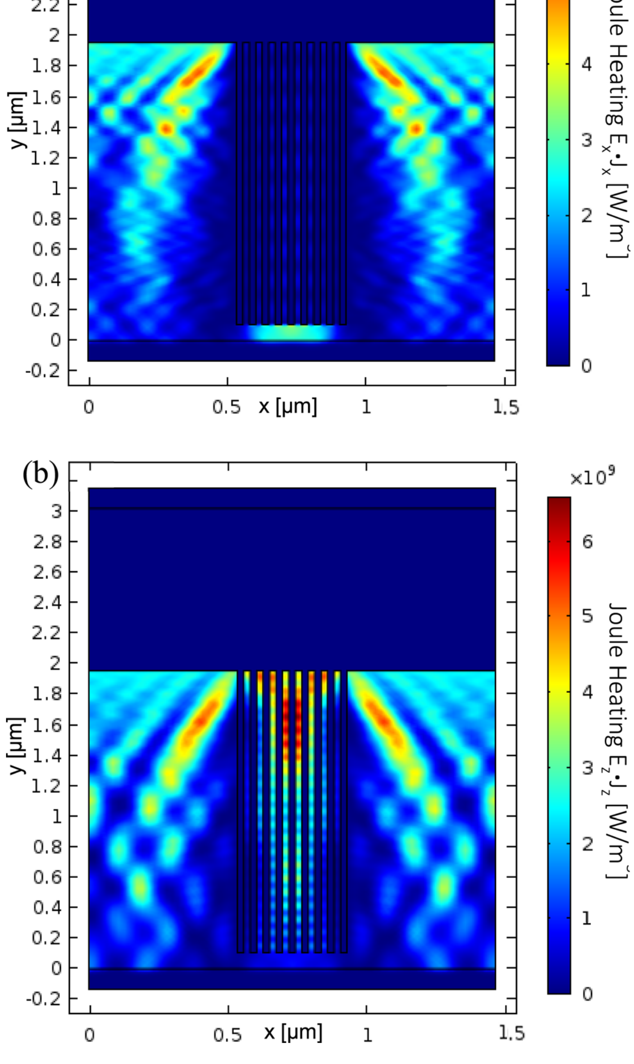

FIG. 8. (Color online) Frequency domain simulations of a 532 nm beam incident on a 22 nm half-pitch, nine trench array with AR = 80. Resistive losses of (a) x- and (b) z-polarized waves are plotted, aligning with the field plots in Fig. 7. Trenches were finely meshed with six elements per opening with an incident field corresponding to 1 W/cm^2 laser fluence. The x-polarized case in (a) shows deep trench power delivery, while the z-polarized case in (b) rapidly dissipates heat at the top of the features.

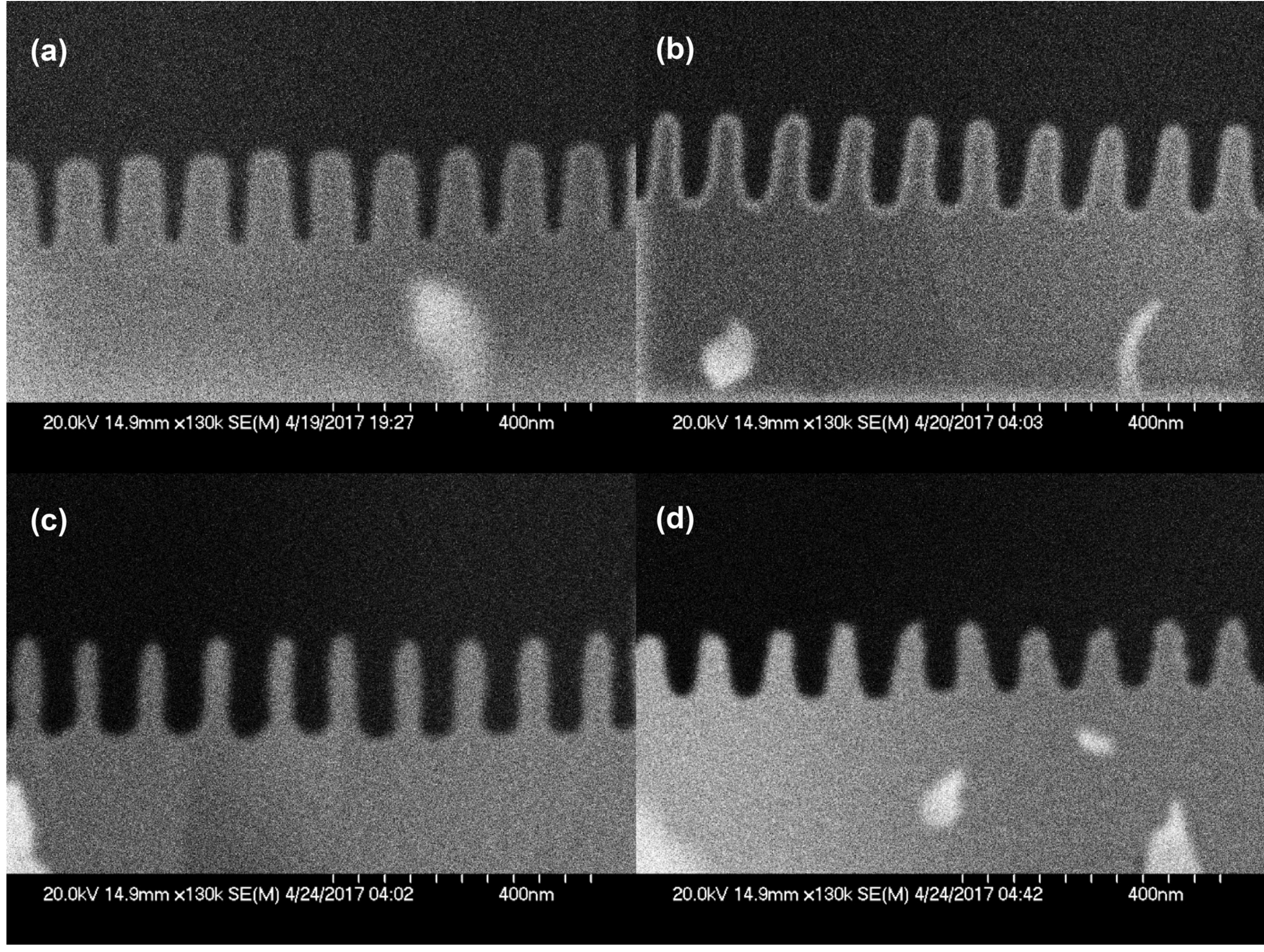

FIG. 9. Cross-sectional SEM images of (a) Si line trench profile pre-etch, (b) postetch (60 s of 50:1 sccm Ar/SF_6 at 9 mTorr, 100 W ICP, 17 cm downstream from the ICP), (c) postetch with 40 mJ/cm^2/pulse 532 nm laser with polarization perpendicular to the trench line, and (d) postetch with 40 mJ/cm^2/pulse 532 nm with polarization parallel to the trench line.

profile postetch with and without laser exposure is pictured in the cross-SEM images of Fig. 9. From the pre-existing trench structure in Fig. 9(a) to postetch in Fig. 9(b), this brief, dilute etch was chosen because of the absence of a hardmask on the patterned wafers. As expected with no substrate bias in an SF_6-containing discharge, chemical etching of the sidewalls has reduced the critical dimension of the trench from 65 ± 5 to 50 ± 3 nm, while the depth remains generally the same due to etching of both the top and bottom of the features.

With the 100 Hz 532 nm Nd:YAG laser introduced at 40 mJ/cm^2/pulse for the duration of the etch, Fig. 9 shows the evolution of the trench profile when laser polarization is applied Fig. 9(c) perpendicular to the trench line (horizontal) and Fig. 9(d) parallel to the trench line (out of page). It is seen that while the perpendicular case in Fig. 9(c) continues with an anisotropic etch, deepening the profile from 120 ± 2 to 140 ± 5 nm and slightly undercutting at the trench base, the parallel polarization case in d) significantly degraded the profile postetch to 90 ± 10 nm, tapering the sidewalls. As predicted by the wave optics simulations in Fig. 8, appreciable power delivery to the trench base encouraged the anisotropy through etch product desorption by targeted hating, while the topical heating caused by the parallel polarization case aggressively etched away the pattern.

IV. CONCLUSIONS

A laser-assisted plasma etching process was presented for visible light (532 nm) on Si at room temperature, showing a minimum intensity of etch onset depending on the polymer deposition in fluorocarbon etch recipes (Fig. 2). This laser-plasma process showed advantages over RIE regarding low surface damage. Through SIMS depth profile data, the Si surface remained pristine under laser exposure midetch on the order of the resolution of the SIMS tool (0.8 nm), while ion bombardment with -140 V DC self-bias created a noticeable Si straggle over 3.5 nm (Fig. 4). Similarly, laser-assisted etching exhibited low incorporation of etch gas residuals (C/F/O) into the Si compared to RIE for the same recipe.

Following predictive modeling of 532 nm light normally incident on 22 nm trench features, the trait of light penetration being highly selective of polarization was shown (Figs. 7 and 8). This effect was confirmed under brief etching conditions in Si linear trenches of $\sim$50 nm half-pitch, with polarization perpendicular to the trench line promoting desorption

of material at the trench base through instantaneous surface heating (Fig. 9).

While these results are notable, the polarization selectivity aspect for deep-trench heating/etching could be perceived as a hinderance to full-wafer processing, as a complex pattern does not consist exclusively of parallel lines. However, laser-assisted etching may be beneficial to etch patterns with features larger than the chosen wavelength, or in simple patterns such as quantum well heterostructures or through-silicon vias for flash memory contacts. The polarization inhomogeneity could even be utilized through appropriate chip design to enable differing etch needs for different regions on a given die.

ACKNOWLEDGMENTS

This work benefited greatly by a gift from the Lam Research Foundation. Surface characterization techniques were mostly carried out at the Frederick Seitz Materials Research Laboratory Central Research Facilites at the University of Illinois Urbana-Champaign, with occasional support and advice from their staff.

[1]International SEMATECH, *International Technology Roadmap for Semiconductors* (The Semiconductor Industry Association, Austin, TX, 2009).
[2]G. Moore, Electronics **38**, 8 (1965).
[3]C. T. Carver, C. T. Carver, J. J. Plombon, P. E. Romero, S. Suri, T. A. Tronic, and R. B. Turkot, Jr., ECS J. Solid State Sci. Technol **4**, N5005 (2015).
[4]H. Shin, W. Zhu, V. M. Donnelly, and D. J. Economou, J. Vac. Sci. Technol., A **30**, 021306 (2012).
[5]C. Arnone and G. B. Scelsi, Appl. Phys. Lett. **54**, 225 (1989).
[6]W. Sesselmann, E. Hudeczek, and F. Bachmann, J. Vac. Sci. Technol., B **7**, 1284 (1989).
[7]J. L. Peyre, C. Vannier, D. Riviere, and G. Villela, Appl. Surf. Sci. **36**, 313 (1989).
[8]G. L. Loper, S. H. Suck-Salk, and M. D. Tabat, Appl. Surf. Sci. **36**, 257 (1989).
[9]D. Riedel, J. L. Hernandez-Pozos, and R. E. Palmer, Appl. Phys. A **78**, 381 (2004).
[10]C. H. Choy and K. W. Cheah, Appl. Phys. A **61**, 45 (1995).
[11]A. Kiani, K. Venkatakrishnan, B. Tan, and V. Venkataramanan, Opt. Express **19**, 10834 (2011).
[12]W. Holber, G. Reksten, and R. M. Osgood, Jr., Appl. Phys. Lett. **46**, 201 (1985).
[13]P. Leerungnawarat, H. Cho, S. J. Pearton, C.-M. N. Zetterling, and M. Ostling, J. Electron. Mater. **29**, 342 (2000).
[14]P. A. Maki and D. J. Ehrlich, Appl. Phys. Lett. **55**, 91 (1989).
[15]M. Ishii, T. Meguro, K. Gamo, T. Sugano, and Y. Aoyagi, Jpn. J. Appl. Phys., Part 1 **32**, 6178 (1998).
[16]D. N. Ruzic and J. R. Sporre, "Method of selective etching a three-dimensional structure," U.S. patent 9,171,733 B2 (27 October 2015).
[17]J. A. Peck, "Laser-enhanced plasma etching of semiconductor materials," Ph.D. thesis (Department of Nuclear, Plasma and Radiological Engineering, University of Illinois at Urbana-Champaign, 2017).
[18]J. A. Peck and D. N. Ruzic, "Mechanism behind dry etching of Si assisted by pulsed visible laser," J. Appl. Phys. **122**, 173304 (2017).
[19]J. F. Ziegler, J. P. Biersack, "Transport of ions in matter (TRIM-2010) [Freeware]," https://www.srim.org/
[20]G. E. Jellison, Jr., F. A. Modine, C. W. White, R. F. Wood, and R. T. Young, Phys. Rev. Lett. **46**, 1414 (1981).